Different trends between extreme and median surface aerosol extinction coefficients over China inferred from quality controlled visibility data

Jing Li[1,*], Chengcai Li[1], Chunsheng Zhao[1]

Department of Atmospheric and Oceanic Sciences, School of Physics, Peking University, Beijing, China, 100871

Abstract

Although the temporal changes of aerosol properties have been widely investigated, the majority focused on the averaged condition without much emphasis on the extremes. However, the latter can be more important in terms of human health and climate change. This study uses a previously validated, quality-controlled visibility dataset to investigate the long-term trends (expressed in terms of relative changes) of extreme surface aerosol extinction coefficient (AEC) over China, and compare them with the median trends. Two methods are used to independently evaluate the trends, which arrive at consistent results. The sign of extreme and median trends are generally coherent, whereas their magnitudes show distinct spatial and temporal differences. In the 1980s, an overall positive trend is found throughout China with the extreme trend exceeding the mean trend, except for Northwest China and the North China Plain. In the 1990s, AEC over Northeast and Northwest China starts to decline while the rest of the country still exhibits an increase. The extreme trends continue to dominate in the south while it yields to the mean trend in

the north. After year 2000, the extreme trend becomes weaker than the mean trend overall in terms of both the magnitude and significance level. The annual trend can be primarily attributed to winter and fall trends. The results suggest that the decadal changes of pollution in China may be governed by different mechanisms. Synoptic conditions that often result in extreme air quality changes might dominate in the 1980s, whereas emission increase might be the main factor for the 2000s.

1. Introduction

As a by-product of the rapid industrial and economic development, China has been faced with a serious issue of air pollution. The variability and trends of China's air quality or aerosol properties have become the focus of numerous past studies (*Jinhuan and Liquan*, 2000; *Che et al.*, 2007; *Deng et al.*, 2008; *Streets et al.*, 2008; *Yoon et al.*, 2011; *Guo et al.*, 2011; *Zhang et al.*, 2015). While many of these works reached important conclusions about the temporal evolution of China's pollution, the majority only analyzed the arithmetic means (e.g., monthly or annual means of aerosol optical depth), with little attention paid to the extreme values. However, it is often these extremes that are responsible for many health and climate related aftermaths. Additionally, considering that the distribution of aerosol optical properties, such as aerosol optical depth (AOD) and extinction coefficients, are often highly right-skewed (*O'Neill et al.*, 2000; *Collaud Coen et al.*, 2013; *Yoon et al.*, 2016), analyzing the arithmetic mean tends to discard the large

43 portion of information in the long tails, thus biasing the result. Moreover, as indicated by
44 previous studies, extreme pollution events are often associated with abnormal synoptic
45 conditions (*Zheng et al.*, 2015; *Ye et al.*, 2016), whereas the mean should be more prone
46 to changes in the emission which increases pollution level overall. Therefore, analyzing
47 the changes in both the mean and extreme values would help understand the factors
48 influencing the variability of pollution.

49 For the few studies that did address temporal changes in the percentiles of aerosol
50 loading, usually either satellite or surface based remote sensing measurements are used,
51 such as Aerosol Optical Depth (AOD) retrievals from Moderate Resolution Imaging
52 Spectroradiometer (MODIS, *Sullivan et al.*, 2015) or the Aerosol Robotic Network
53 (AERONET, *Xia*, 2011; *Yoon et al.*, 2016). Nonetheless, remote sensing data is not ideal
54 for extreme analysis, mainly because it frequently misses heavy pollution conditions
55 likely associated with strict cloud screening (*Lin and Li*, 2016). Moreover, remote sensing
56 techniques cannot recognize mixed layer height, a major parameter affecting surface air
57 pollution, which make them unsuitable for air quality studies. As a result, the “real”
58 extremely high aerosol loadings cannot be well detected using remote sensing. On the
59 other hand, surface visibility observations that do not require cloud screening or other
60 retrieval assumptions, can serve as a suitable alternative for pollution related research.
61 After eliminating fog, rain or snow conditions, degradation of surface visibility can be
62 mainly attributed to aerosol extinction and are thus closely related to air quality (*Husar et*
63 *al.*, 2000). Moreover, since routine visibility observation started as early as 1970s for

64 many sites, these data can offer a much longer time series for trend analysis than remote
65 sensing products. Previously, *Li et al.* (2016) used a quality controlled (by comparing
66 against surface PM_{10} and $PM_{2.5}$ measurements) visibility converted Aerosol Extinction
67 Coefficient (AEC) dataset to study temporal changes of monthly mean surface aerosol
68 extinction in China for the past 30 years and found that there are obvious shifts in the
69 trends for different time periods. However, it still remains to understand whether the
70 extreme values change faster or slower than the mean.

71 In this paper, we use the same dataset as in *Li et al.* (2016) to further investigate the
72 trends of extremely high (defined as the 95^{th} percentile) surface aerosol extinction
73 coefficients and compare them with the median trends representing averaged condition.
74 Although a threshold visibility value is often used in previous studies to define extreme
75 events (e.g., *Fu et al.* 2013 define extreme pollution as visibility lower than 5 km
76 conditions), the same threshold does not apply to all sites since their reporting
77 conventions may be different. We thus believe a percentile criterion would be more
78 appropriate. In addition to estimating the linear trend of the 95^{th} percentile value itself, we
79 also use a novel method proposed by *Franzke* (2013) based on quantile regression with
80 surrogate data testing for significance, who used this method to test for significant trends
81 in extreme temperatures. To our knowledge, this method has not been applied to aerosol
82 related research, and the independent application of two methods increases the robustness
83 of the results.

84 In section 2, we describe the data and method used in this study. The analysis results

85 are presented in section 3, followed by the conclusions and a brief discussion in section 4.

86

87 **2. Data and Methods**

88

89 **2.1 Visibility data**

90

91 Here we use the same visibility dataset as in *Li et al.* (2016). This hourly surface
92 visibility dataset is obtained from the National Centers for Environmental Information
93 (NCDC, http://www1.ncdc.noaa.gov/pub/data/noaa/) of the National Oceanic and
94 Atmospheric Administration (NOAA). The data selection criteria and quality control
95 procedure strictly follows those implemented by *Li et al.* (2016). Briefly, data before
96 1980 is not used because of different reporting standard (*Che et al.*, 2007; *Wu et al.*,
97 2012). Those after 2013 are also excluded because many sites have replaced human
98 observation with automatic visibility sensors. Then the eight quality assurance steps
99 proposed by *Li et al.* (2016) is applied to the dataset. A total of 272 sites are selected for
100 China, whose data have been manually inspected to show no observable jumps or spikes.
101 The visibility is further converted to Aerosol Extinction Coefficient (AEC) using the
102 Koschmieder formula (*Koschmieder*, 1926), and corrected for relative humidity effects
103 according to *Husar and Holloway* (1984) and *Che et al.* (2007). This AEC dataset has
104 also been validated against surface $PM_{2.5}$ and PM_{10} measurements. Please refer to *Li et al.*
105 (2016) for detailed description of the correction and validation processes.

106

107 **2.2 Trend analysis methods**

108

109 We define extremes as the 95th percentile of the visibility converted surface AEC.
110 The hourly AEC is first averaged to daily values and 95th percentile (50th percentile for
111 the median trend) is then calculated for each year or each season for the seasonal analysis.
112 To estimate trend of the extremes, we use two independent methods. The first is to obtain
113 an annual or seasonal time series of the 95th percentile of the extinction coefficients and
114 then perform a *Sen*'s slope (*Sen*, 1968) estimate of its linear trend. The *Sen*'s slope *b* is
115 calculated as

116 $$b = \text{Median}(\frac{X_i - X_j}{i - j}) \forall j < i \quad (1)$$

117 where X_i and X_j are the *i*th and *j*th value in the time series respectively.

118 Then the Mann-Kendall statistical test (*Mann*, 1945; *Kendall*, 1975) is applied to test
119 whether the trend is significant at 95% level. The test statistic is calculated as

120 $$S = \sum_{i=1}^{n-1} \sum_{j=i+1}^{n} \text{sgn}(X_j - X_i) \quad (2)$$

121 Where n is the number of data points, and sgn is the sign function:

122 $$\text{sgn}(X_j - X_i) = \begin{cases} +1 & \text{if} \quad X_j > X_i \\ 0 & \text{if} \quad X_j = X_i \\ -1 & \text{if} \quad X_j < X_i \end{cases} \quad (3)$$

123 The variance of *S* is given by

$$\mathrm{Var}(S) = \frac{1}{18} n(n-1)(2n+5) \tag{4}$$

If the sample size n>30, which is well satisfied in our case, the standard normal test statistic ZS is computed using:

$$ZS = \begin{cases} \dfrac{S-1}{\sqrt{\mathrm{Var}(S)}} & \text{if } S>0 \\ 0 & \text{if } S=0 \\ \dfrac{S+1}{\sqrt{\mathrm{Var}(S)}} & \text{if } S<0 \end{cases} \tag{5}$$

According to the normal distribution table, the 5% significance level is satisfied if $|ZS|>1.96$.

The second approach is quantile regression, which is a well established method used in many previous studies (*Koenker and Hallock*, 2001; *Hannachi*, 2006; *Barbosa et al.*, 2011; *Donner et al.*, 2012; *Franzke*, 2013) to estimate extreme trends of climate data.

For regular linear least square regression, the model can be expressed as

$$E[y \mid \mathbf{X}] = \beta \mathbf{X} + \varepsilon \tag{6}$$

where y is the response variable conditioned on $\mathbf{X}$, and the β's satisfy the minimization of the summed error function

$$err = \min \sum_i \xi(y_i - \beta X_i) \tag{7}$$

where

$$\xi(u) = u^2 \tag{8}$$

For linear quantile regression, the response variable becomes the τ th ($\tau \in [0,1]$) quantile of y conditioned on $\mathbf{X}$,

142 $$Q_\tau[y \mid \mathbf{X}] = \beta\mathbf{X} + \varepsilon \quad (9)$$

143 where the βs still satisfy equation (2), but equation (3) now becomes

144 $$\xi_\tau(u) = \begin{cases} u\tau & u \geq 0 \\ u(\tau - 1) & u < 0 \end{cases} \quad (10)$$

145 Note that ξ_τ is symmetric when $\tau = 0.5$, rotated to the right when $\tau < 0.5$ and to the
146 left when $\tau > 0.5$. The quantile regression problem can be numerically solved by linear
147 programming (*Koenker and Hallock*, 2001). Here we use the R package "quantreg" to
148 solve for the regression coefficients of daily mean AEC. Trends for both the 95th and 50th
149 (median) percentiles are estimated and the trends are compared. To test for significance of
150 the quantile regression trends, we adopt the bootstrap approach proposed by *Franzke*
151 (2013), who used surrogate data generated with the same autocorrelation function and the
152 same probability density function as the original dataset. The detailed generation
153 procedure can be found in *Schreiber and Schmitz* (1996) and *Franzke* (2013). Here we
154 generate 1000 surrogate time series to represent the intrinsic variability of the AEC time
155 series.

156 In addition, we also calculate the trends for the median AEC (50th percentile) using
157 the above two methods, and compare them with the extreme trends. All trends are
158 normalized and expressed as relative changes per decade, calculated as trend slope times
159 the length of the time series divided by the corresponding AEC percentiles of the initial
160 year. Therefore the trends reported are unitless.

161 Figure S1 in the supplement shows an example of the trend analysis using these two

methods. In the following text, to save space we only present trends using quantile regression, whereas the *Sen's* slope results, which agree well with the former, are presented in the supplement material.

3. Results

3.1 Trend Maps

We first examine the distribution and temporal changes of trends for all sites in China. As indicated by *Li et al.* (2016), there are significant temporal shifts of the magnitude and sign of monthly mean AEC trends for different decades. We thus also respectively examine the extreme and median trends for three consecutive decades: 1980-1990, 1991-2000 and 2000-2013. The overall trends for the 1980 to 2013 period are weakly positive for the majority of the sites (see Figure S2).

The three columns in Figure 1 show the distribution of extreme trend (upper row), median trend (middle row) and their differences (extreme minus median, bottom row) for the 272 sites for the three periods respectively. To avoid the confusion caused by positive and negative signs of the trend, the difference here are calculated using the absolute value of the extreme and median trends. Larger dots in black circles mean that the trends are statistically significant at 95% level. Figure 1 is the results from quantile regression, whereas the trends using *Sen*'s slope is presented in Figure S3, which shows largely

183 consistent pattern. It is seen from Figure 1 that the sign of median and extreme trends
184 mostly agree throughout China. An extensive positive trend is observed all over China in
185 the 1980s. During the 1990s, many sites, especially those in north China, began to
186 experience a decreased AEC. After year 2000, the north China sites continue to show
187 decreasing trends whereas AEC over many south China sites started to rise again.

188 However, a detailed comparison between median and extreme trends reveals distinct
189 spatial and temporal differences. Focusing on the bottom three panels of Figure 1 (g-h), it
190 is clear that in the 1980s, the extreme trends exceed the median trend throughout China,
191 with some differences as large as 50% (northwestern sites). The number of sites showing
192 significant extreme trend (178) is also greater than those with significant median trend
193 (91). Note that the number of significant sites can be different between quantile
194 regression and *Sen*'s slope results, because (1) quantile regression is applied to daily data
195 while *Sen*'s slope uses annual or seasonal percentiles and (2) quantile regression uses
196 bootstrap method to test for significance while *Sen*'s slope uses MK test. Nonetheless, the
197 spatial patterns of the two methods are consistent. In the 1990s, the distribution of the
198 trend differences switched to a north-south "dipole" pattern, with negative values in the
199 north and positive in the south in general, i.e., extreme trends are weaker than the median
200 trend in the north but stronger in the south, with a rough separation at 33°N marked by
201 the horizontal black line on Figure 1h. In the north, the sites showing significant extreme
202 trends also becomes fewer than those with significant median trends in the north. Even in
203 the south, the difference between the extreme and median trends is much smaller

compared to the 1980s, indicating a slowdown of the increase in the extreme values. After year 2000, almost the entire China exhibits a "blue" pattern as opposed to the "red" pattern in the 1980s. Except for a few sites in central south China, the majority exhibits a weaker extreme trend than the mean trend. There are also fewer sites showing significant trends in the extreme (52) than in the median (119). This feature is particularly strong for northeast, northwest and south China. Although east and south China still show positive AEC trends, this result suggest that in this decade, the extreme pollution conditions have not increased as much as the mean or background pollution.

In short, the positive trends in the 1980s over China can be primarily attributed an increase in the extremes. The 1990s experienced with a transition, with extreme trends becoming weaker than the median trend in the north and only slightly stronger in the south. Finally in the 2000s, the extreme trends largely yield to the median trends.

3.2 Regional Trends

To examine the spatial and temporal changes in more detail, we further divide the country into six representative regions, marked by black rectangles on Figure 1b. Three of these regions: the North China Plain (NCP), Yangtze River Delta (YRD), and Pearl River Delta (PRD) are the major urban conglomerates in China. Since the change in the extreme and median is essentially related to the shift of the distribution, we first evaluate the regional AEC ($/Mm^{-1}$) distributions for the three decades. Figure 2 plots these

distributions by region on logarithmic scale, as AEC is usually considered to follow a lognormal distribution (*Collaud Coen et al.*, 2013). The dashed lines in Figure 2 indicate location of the 95th percentile. For all regions, there is a rightward extension of the tail of the distribution from 1990s to 1980s, implying an increase of the extremes, which is also characterized by the rightward shift of the 95th percentile line. NCP, YRD and NW China also show a rightward shift of the distribution peak. From 1990s to 2000s, although the distribution peak shifts to the right for PRD, YRD, SW China and NE China, there is no obvious shift in the tail for these four regions. For the other two regions, NCP and NW China, there is a leftward shift in both the peak and the tail, but the shift of the peak is stronger. Overall, we can roughly conclude that the 1980s' AEC trend is characterized by a change of the extremes, while in the 2000s the median dominates the trend.

Consistent with *Li et al.* (2016), we also calculate trends successively for all periods starting each year from 1980 to 2004 and ends in 2013 with 10-year increments. Figure 3 shows the temporal evolution of the quantile regression trend differences with x axis indicating the trend calculation start year and y axis indicating the length of the time series, with its counterpart using *Sen's* slope shown by Figure S4. To save space, only the absolute differences between the extreme and median trends are presented in Figure 3, while their respective values are shown in Figures S5 and S6 for quantile regression and Figures S7 and S8 for *Sen*'s slope. Table 1 displays the regional extreme and median trends using the two methods and their differences for the three periods: 1980-1990, 1991-2000, 2001-2013. Note although the absolute values of Sen's slope and quantile

246 regression trends can be different, their signs are consistent. The time series and linear
247 trends for each region are presented in Figure S9. Because in Figure 3 the trends are
248 calculated successively for each period, it helps to examine the time node of the changes
249 more precisely. For example, although Figures 1 and 2 both indicate that the extremes
250 increase more rapidly in the 1980s, for YRD and PRD, the duration is short with the
251 extreme trend exceeding the median trend since around 1982, while for the rest four
252 regions the change happened around 1986 or later. YRD, PRD and NE China experienced
253 a short period of stronger extreme trend from ~1994 to 1996, whereas the other three
254 regions show weaker extreme trends. After 2002, SW and NW China display a slightly
255 higher extreme trend, which is different from the rest four regions. These features suggest
256 that there can be minor differences when the trends are examined for different time
257 periods.

258 The seasonal time series of the difference between extreme and median quantile
259 regression trends are plotted in Figure 4, with a 4-year moving average to smooth out
260 small wrinkles (its counterpart using *Sen*'s slope is shown in Figure S10). Note that
261 Figure 4 shows the evolution of the trend difference for every ten-year period from 1980
262 to 2004 (i.e, 1980-1989, 1981-1990,…, 2004-2013). An outstanding feature in Figure 4 is
263 that for all regions, the summer (JJA) trend difference (indicated by red curves) exhibit
264 quite different, or even reversed variability from the other three seasons and the annual
265 result. For NE, NW China and the PRD, spring (MAM) trends also have relatively larger
266 departure. In general, winter (DJF) and fall (SON) trends agree better with the annual

267 trend. Since these two seasons are dominated by anthropogenic aerosols such as sulfate,
268 nitrate, black and organic carbon throughout China (*Cao et al.*, 2007; *Wang et al.*, 2007;
269 *Wang et al.*, 2015), the results indicate that changes in anthropogenic aerosol loading are
270 primarily responsible for the observed extreme and median trends. In the spring many
271 regions are influenced by dust, and in the summer, the relative humidity effect may
272 significantly enhance aerosol extinction. Both are natural factors and should have minor
273 contribution to the annual trend according to Figure 4.
274
275 **4. Conclusions and Discussion**
276
277 While the trends of aerosol pollution in China have been studied extensively, it
278 remains to understand whether the extreme conditions have changed and whether their
279 changes are faster or slower than the mean. In this study, we use a quality controlled
280 visibility dataset to examine decadal trends of extreme values of surface aerosol
281 extinction coefficients. Quantile regression and *Sen*'s slope estimates are jointly used to
282 estimate the trends to improve its robustness. Our analysis reveals that in general, the
283 extreme and median trends agree in terms of the sign, but they can differ significantly in
284 terms of the amplitude. During the 1980s, the extremes increased faster than the median
285 for most China except for a few north and northwest sites. The 1990s experienced a
286 transition with extreme trend becoming weaker than median trend in the north but still
287 slightly stronger in the south. Then in the 2000s, the majority of the country exhibited a

288 weaker extreme trend than the median trend. Seasonally, winter and fall trends are the
289 most consistent with annual trends, while the summer trend shows the largest departure
290 from the annual trend.

291 This study uses daily mean daytime AEC without accounting for its diurnal
292 variability. Nonetheless, visibility can still change considerably in the course of a day
293 (*Deng et al.*, 2011). To examine this effect we repeat the analysis using daily minimum
294 and daily maximum AEC respectively. Their counterparts of Figure 1 are shown in
295 Figures S11 and S12. A brief comparison indicates high resemblance of these two figures
296 to Figure 1 that uses daily mean data, albeit with some reasonable differences in the
297 amplitude.

298 The reason for the different behaviors between the extreme and median trends still
299 needs further investigation, and will be the topic of our future study. Some implication is
300 that in the 1980s and part of 1990s, synoptic conditions might be playing a major role in
301 modulating aerosol variability. For example, several extremely heavy pollution events are
302 believed to be linked to stagnant weather (*Tao et al.*, 2014; *Zheng et al.*, 2015). After mid
303 1990s, emission might become more dominate which tends to increase both the extreme
304 and the mean. But since it is a relatively uniform background change, the signal might be
305 more prominent in the mean condition. On the other hand, aerosol properties can also be
306 potentially influenced by decadal or interannual climate variability (*Chen and Wang*,
307 2015; *Wang and Chen*, 2016), whose footprint may be embedded in these extreme and
308 mean trends. However, the mechanism that they impact on the extremes and the mean

still need to be understood, and likely require a comprehensive study using both observations and model simulations. This also requires the models to accurately simulate the extreme events, which is a challenging task.

Admittedly, the visibility data is not ideal for aerosol-related studies, given its various sources of uncertainties as discussed in *Li et al.* (2016). However, it is a currently best compromise since there is lack of reliable long-term aerosol observation datasets. Moreover, remote sensing produces are vulnerable to extreme pollution, making them unsuitable for extreme trend studies. For example, as discussed in *Lin and Li* (2013), MODIS frequently misses the heavy haze over north China likely due to cloud screening algorithm. Sun photometers will also stop working when the sun is blocked by the heavy pollution. This also suggests that current remote sensing instruments and retrieval algorithms need to be improved to observe these extreme events.

Acknowledgements

We thank the NOAA NCDC database for providing the hourly visibility measurements used for this study. The data is downloaded from the NCDC public ftp at http://www1.ncdc.noaa.gov/pub/data/noaa/. This work is funded by National Science Foundation of China Grants No. 41575018 and No. 41530423, and the 1000-Young Talent program of China.

References

330

331 Barbosa, S. M. (2011), Testing for Deterministic Trends in Global Sea Surface
332 Temperature, *J. Climate*, *24*, 2516–2522, doi:10.1175/2010JCLI3877.1.
333 Cao, J. J., et al. (2007), Spatial and seasonal distributions of carbonaceous aerosols over
334 China, *J. Geophys. Res.*, 112, D22S11, doi:10.1029/2006JD008205.
335 Che, H., X. Zhang, Y. Li, Z. Zhou, and J. J. Qu, (2007). Horizontal visibility trends in
336 China 1981–2005. *Geophys. Res. Lett.*, *34*(24).
337 Chen, H. P., and H. J. Wang (2015), Haze days in North China and the associated
338 atmospheric circulations based on daily visibility data from 1960 to 2012. *J. Geophys.*
339 *Res. Atmos.*, 120(12), 5895-5909.
340 Collaud Coen, M., Andrews, E., Asmi, A., Baltensperger, U., Bukowiecki, N., Day, D.,
341 Fiebig, M., Fjaeraa, A. M., Flentje, H., Hyvärinen, A., Jefferson, A., Jennings, S. G.,
342 Kouvarakis, G., H. Lihavainen, C. Lund Myhre, W. C. Malm, N. Mihapopoulos,
343 J.V. Molenar, C. O'Dowd, J. A. Ogren, B. A. Schichtel, P. Sheridan, A. Virkkula, E.
344 Weingartner, R. Weller, P. and Laj, P. (2013), Aerosol decadal trends – Part 1: In-situ
345 optical measurements at GAW and IMPROVE stations, *Atmos. Chem. Phys.*, 13,
346 869-894, doi:10.5194/acp-13-869-2013.
347 Deng, J., T. Wang, Z. Jiang, M. Xie, R. Zhang, X. Huang, and J. Zhu (2011).
348 Characterization of visibility and its affecting factors over Nanjing, China. *Atmos.*
349 *Res.*, *101*(3), 681-691.
350 Deng, X., X. Tie, D. Wu, X. Zhou, X. Bi, H. Tan, F. Li and C. Jiang (2008). Long-term

351 trend of visibility and its characterizations in the Pearl River Delta (PRD) region,
352 China. *Atmos. Environ.*, *42*(7), 1424-1435.
353 Donner, R. V., R. Ehrcke, S. M. Barbosa, J. Wagner, J. F. Donges, and J. Kurths (2012),
354 Spatial patterns of linear and nonparametric long-term trends in Baltic sea-level
355 variability, *Nonlin. Processes Geophys.*, *19*, 95–111, doi:10.5194/npg-19-95-2012.
356 Fu, C., Wu, J., Gao, Y., Zhao, D., and Han, Z. (2013). Consecutive extreme visibility events
357 in China during 1960–2009. *Atmos. Environ.*, *68*, 1-7.
358 Franzke, C. (2013), A novel method to test for significant trends in extreme values in
359 serially dependent time series, *Geophys. Res. Lett.*, 40, 1391–1395,
360 doi:10.1002/grl.50301.
361 Guo, J. P., X. Y. Zhang, Y. R. Wu, Y. Zhaxi, H. Z. Che, B. La, W. Wang and X. W. Li,
362 (2011). Spatio-temporal variation trends of satellite-based aerosol optical depth in
363 China during 1980–2008. *Atmos. Environ.*, *45*(37), 6802-6811.
364 Hannachi, A. (2006), Quantifying changes and their uncertainty in probability
365 distributions of climate variables using robust statistics, *Clim. Dyn.*, *27*, 301–317,
366 doi:10.1007/s00382-006-0132-X.
367 Husar, R. B., and J. M. Holloway (1984), The properties and climate of atmospheric haze,
368 in Hygroscopic Aerosols, edited by L. H. Ruhnke and A. Deepak, pp. 129–170,
369 *Deepak Publ.,* Hampton, Va.
370 Husar, R. B., J. D. Husar, and L. Martin (2000). Distribution of continental surface aerosol
371 extinction based on visual range data. *Atmos. Environ.*, *34*(29), 5067-5078.

372 Jinhuan, Q., and Liquan, Y. (2000). Variation characteristics of atmospheric aerosol optical
373 depths and visibility in North China during 1980–1994. *Atmos. Environ.*, *34*(4),
374 603-609.
375 Kendall, M. G. (1975), Rank Correlation Methods, *Griffin*, London.
376 Koenker, R., and K. F. Hallock (2001), Quantile regression, *J. Economic Prespectives*, *15*,
377 143–156.
378 Koschmieder, H. (1926). Theorie der horizontalen Sichtweite. *Beitsaege Physik zur*
379 *Atmosphere* 12, 33-55.
380 Li, J., C. Li, C. Zhao, and T. Su (2016), Changes in surface aerosol extinction trends over
381 China during 1980–2013 inferred from quality-controlled visibility data, *Geophys. Res.*
382 *Lett.*, 43, 8713–8719, doi:10.1002/2016GL070201.
383 Lin, J.-T., and J. Li (2016), Spatio-temporal variability of aerosols over East China inferred
384 by merged visibility-GEOS-Chem aerosol optical depth, *Atmos. Environ.*, 132, 111-122,
385 doi:doi:10.1016/j.atmosenv.2016.02.037.
386 Mann H. B. (1945). Nonparametric tests against trend. *Econometrica* **13**: 245–259.
387 O'Neill, N. T., A. Ignatov,B. N. Holben, and T. F. Eck (2000). The lognormal distribution
388 as a reference for reporting aerosol optical depth statistics; Empirical tests using
389 multi-year, multi-site AERONET sunphotometer data. *Geophys. Res. Lett*, *27*(20),
390 3333-3336.
391 Schreiber, T., and A. Schmitz (1996), Improved surrogate data for nonlinearity tests,
392 *Phys. Rev. Lett.*, 77, 635–638.

393 Sen, P. K. (1968), Estimates of the regression coefficient based on Kendall's tau, *J. Am.,*
394 *Stat. Assoc.*, 63, 1379–1389.
395 Streets, D. G., C. Yu, Y. Wu, M. Chin, Z. Zhao, T. Hayasaka and G. Shi (2008). Aerosol
396 trends over China, 1980–2000. *Atmos. Res.*, *88*(2), 174-182.
397 Sullivan, R. C., R. C. Levy and S. C. Pryor (2015). Spatiotemporal coherence of mean and
398 extreme aerosol particle events over eastern North America as observed from
399 satellite. *Atmos. Environ.*, *112*, 126-135.
400 Tao, M., L. Chen, X. Xiong, M. Zhang, P. Ma, J. Tao and Z. Wang (2014). Formation
401 process of the widespread extreme haze pollution over northern China in January 2013:
402 Implications for regional air quality and climate. *Atmos. Environ.*, *98*, 417-425.
403 Wang, G., K. Kawamura, X. Zhao, Q. Li, Z. Dai and H. Niu (2007). Identification,
404 abundance and seasonal variation of anthropogenic organic aerosols from a mega-city in
405 China. *Atmos. Environ.*, *41*(2), 407-416.
406 Wang, Q. Y., R.-J. Huang, J. J. Cao, X. X. Tie, H. Y. Ni, Y. Q. Zhou, Y. M. Han, T. F. Hu, C.
407 S. Zhu, T. Feng, N. Li, and J. D. Li (2015), Black carbon aerosol in winter northeastern
408 Qinghai–Tibetan Plateau, China: the source, mixing state and optical property, *Atmos.*
409 *Chem. Phys.*, 15, 13059-13069, doi:10.5194/acp-15-13059-2015.
410 Wang, H. J. and H. P. Chen (2016), Understanding the recent trend of haze pollution in
411 eastern China: roles of climate change. *Atmos. Chem. Phys.*, 16, 4205-4211.
412 Wu, J., C. Fu, L. Zhang and J. Tang, J. (2012). Trends of visibility on sunny days in China
413 in the recent 50 years. *Atmos. Environ.*, *55*, 339-346.

414 Xia, X. (2011). Variability of aerosol optical depth and Angstrom wavelength exponent
415 derived from AERONET observations in recent decades. *Environ. Res. Lett.*, *6*(4),
416 044011.
417 Ye, X., Y. Song, X. Cai and H. Zhang (2016). Study on the synoptic flow patterns and
418 boundary layer process of the severe haze events over the North China Plain in January
419 2013. *Atmos. Environ.*, *124*, 129-145.
420 Yoon, J., W. von Hoyningen-Huene, M. Vountas and J. P. Burrows (2011), Analysis of
421 linear long-term trend of aerosol optical thickness derived from SeaWiFS using BAER
422 over Europe and South China, *Atmos. Chem. Phys.*, 11, 12149-12167,
423 doi:10.5194/acp-11-12149-2011, 2011.
424 Yoon, J., A. Pozzer, D. Y. Chang, J. Lelieveld, J. Kim, M. Kim, Y. G. Lee, J.-H. Koo and K.
425 J. Moon (2016). Trend estimates of AERONET-observed and model-simulated AOTs
426 between 1993 and 2013. *Atmos. Environ.*, *125*, 33-47.
427 Zhang, X., L. Wang, W. Wang, D. Cao, X. Wang and D. Ye (2015). Long-term trend and
428 spatiotemporal variations of haze over China by satellite observations from 1979 to
429 2013. *Atmos. Environ.*, *119*, 362-373.
430 Zheng, G. J., F. K. Duan, H. Su, Y. L. Ma, Y. Cheng, B. Zheng, Q. Zhang, T. Huang, T.
431 Kimoto, D. Chang, U. Pöschl, Y. F. Cheng and K. B. He (2015), Exploring the severe
432 winter haze in Beijing: the impact of synoptic weather, regional transport and
433 heterogeneous reactions, *Atmos. Chem. Phys.*, 15, 2969-2983,
434 doi:10.5194/acp-15-2969-2015.

435 Table 2. Regional extreme and median trends

Region	1980-1990						1991-2000						2001-2013					
	SL* 95th percentile	SL Median	Difference	QR* 95th percentile	QR Median	Difference	SL* 95th percentile	SL Median	Difference	QR* 95th percentile	QR Median	Difference	SL* 95th percentile	SL Median	Difference	QR* 95th percentile	QR Median	Difference
NE China	.97	.73	.24	.87	.58	.29	-.26	-.27	.02	-.24	-.31	.08	-.16	-.13	-.03	-.16	-.22	.06
NCP	.67	.70	-.03	.59	.71	-.11	-.14	-.02	-.12	-.13	-.17	.04	.15	.27	-.12	.16	.28	-.12
NW China	.88	.79	.11	.91	.87	.04	.12	-.19	.32	-.01	-.22	.21	-.15	-.23	.08	-.09	-.24	.15
SW China	.55	.15	.40	.46	.13	.33	.04	-.03	.07	.00	-.05	.05	.19	.07	.12	.16	.07	.09
YRD	.68	.32	.36	.59	.33	.26	.05	-.11	.16	.08	-.02	.10	.13	.32	-.19	.14	.33	-.19
PRD	.76	.17	.59	.66	.18	.48	.16	.12	.05	.13	.07	.06	.43	.54	-.11	.40	.53	-.13

436 * SL refers to Sen's slope and QR refers to quantile regression

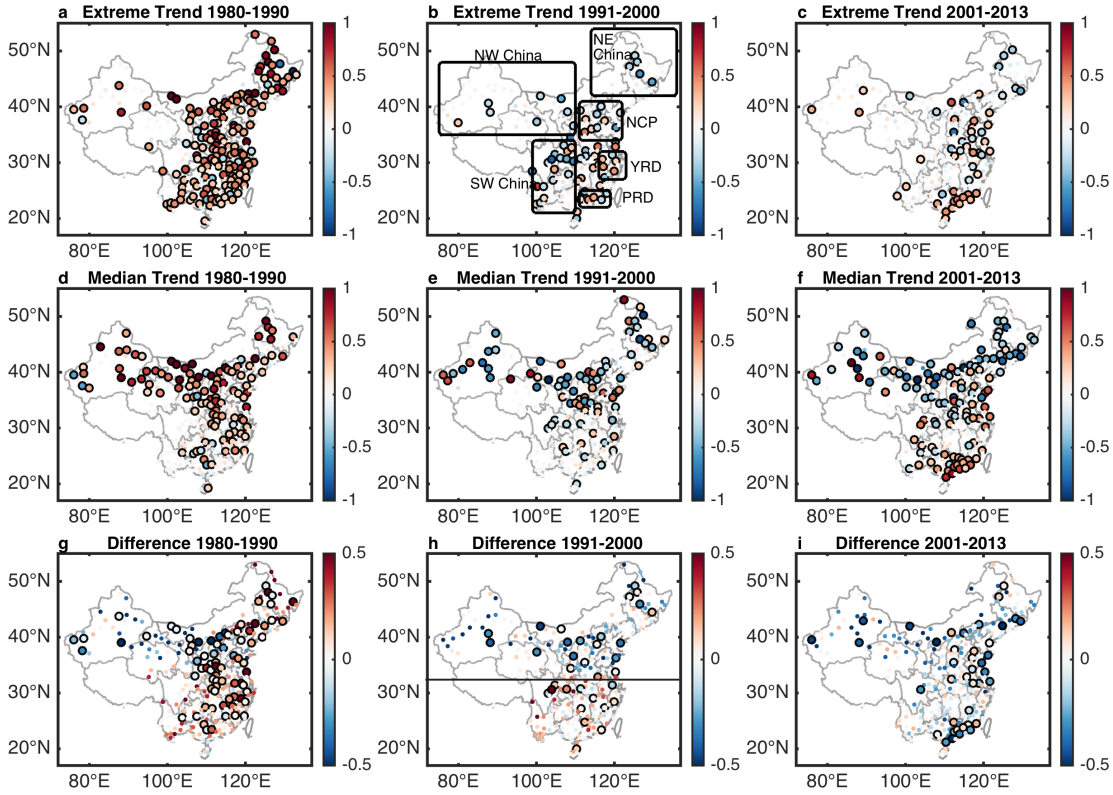

437

438 **Figure 1.** The first row: extreme trends estimate using quantile regression for the three
439 decades, 1980-1990 (a), 1991-2000 (b), 2001-2013 (c); The second row: median trends
440 estimated using quantile regression for the three decades; Bottom row: the difference
441 between the values of the extreme trends and median trends, calculated as the extreme
442 minus median. All trends are unitless and expressed as relative changes.

443

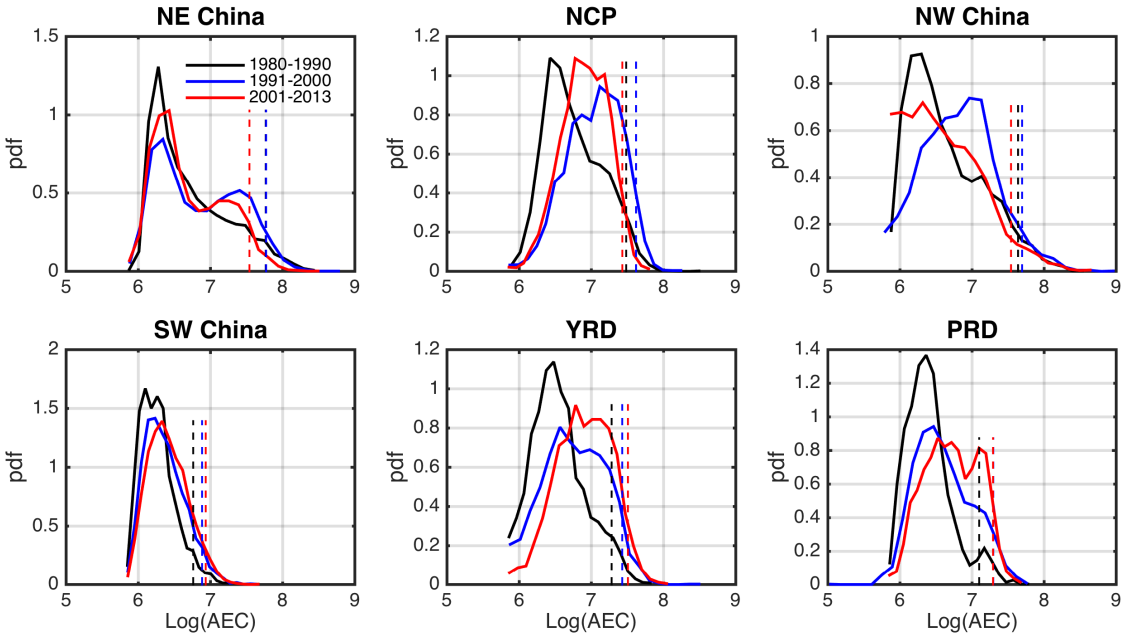

Figure 2. Probability distribution function (pdf) of AEC (megameter^{-1}) for the three decades over the six representative regions marked on panel b of Figure 1. The AEC has been converted to logarithmic scale.

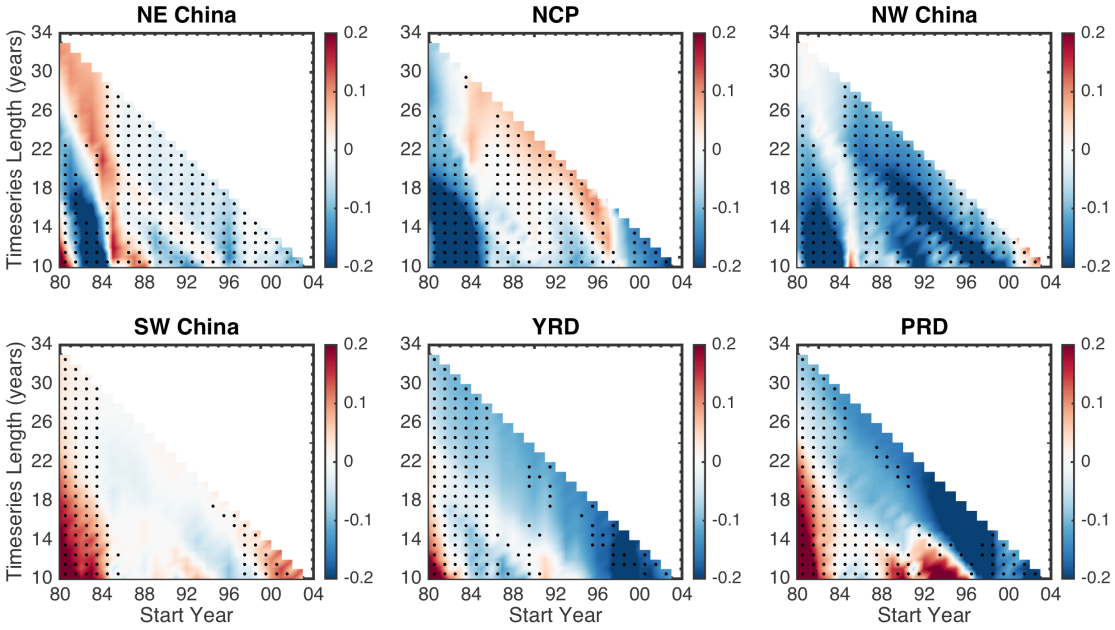

Figure 3. Difference between extreme and median trends calculated using quantile regression for the six representative regions marked on panel b of Figure 1. Trends are between each year from 1980 to 2004 and the end of the record, with 10 minimum. The x axis indicates the staring year, and the y axis indicates the length of the time series to calculate the trend.

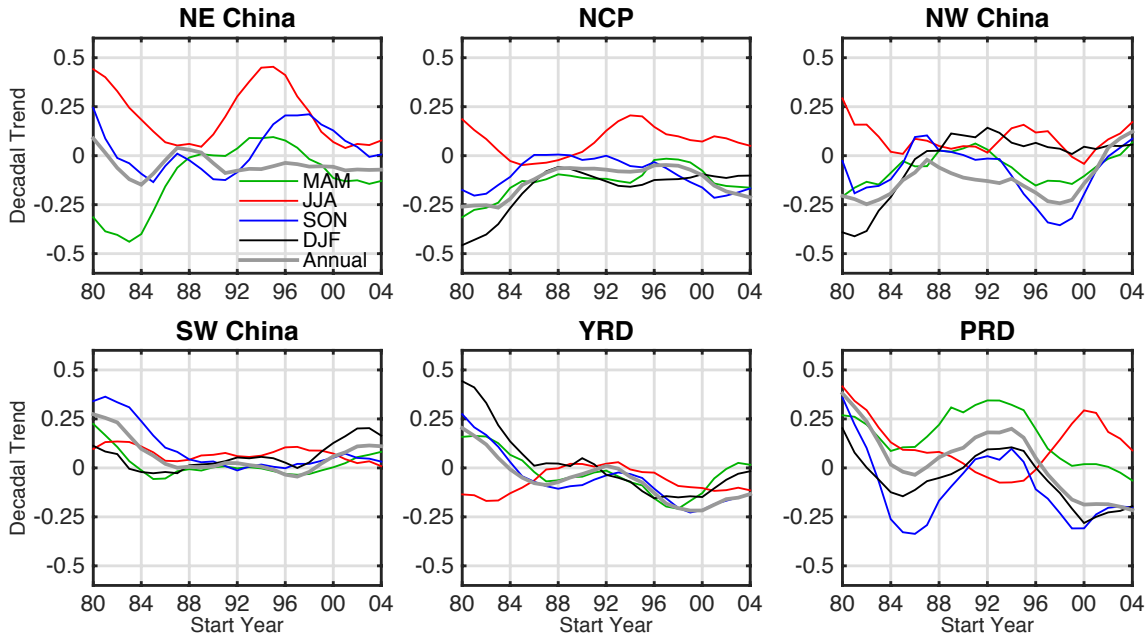

Figure 4. Seasonal time series of the difference between the extreme and median trends. The trends are calculated for each 10 year period starting form 1980 to 2004 (x axis), i.e., the first point is the trend difference for the 1980 to 1989 period, the second from 1982 to 1990, etc.